analytical chemistry

Article

pubs.acs.org/ac

In Vivo Live Cell Imaging for the Quantitative Monitoring of Lipids by Using Raman Microspectroscopy

Masahito Hosokawa,[†,‡,⊥] Masahiro Ando,[‡,⊥] Shoichiro Mukai,[†] Kyoko Osada,[†] Tomoko Yoshino,[†] Hiro-o Hamaguchi,*[,‡,§] and Tsuyoshi Tanaka*[,†,∥]

[†]Division of Biotechnology of Life Science, Institute of Engineering, Tokyo University of Agriculture and Technology, 2-24-16, Naka-cho, Koganei 184-8588, Japan

[‡]Institute for Nanoscience and Nanotechnology, Waseda University, 513, Wasedatsurumaki-cho, Shinjuku-ku, Tokyo 169-8050, Japan

[§]Institute of Molecular Science and Department of Applied Chemistry, National Chiao Tung University, 1001 Ta Hsueh Road, Hsinchu 30050, Taiwan

[∥]Core Research for Evolutional Science and Technology, Japan Science and Technology Agency, 5 Sanbancho, Chiyoda-ku, Tokyo 102-0075, Japan

Supporting Information

ABSTRACT: A straightforward in vivo monitoring technique for biomolecules would be an advantageous approach for understanding their spatiotemporal dynamics in living cells. However, the lack of adequate probes has hampered the quantitative determination of the chemical composition and metabolomics of cellular lipids at single-cell resolution. Here, we describe a method for the rapid, direct, and quantitative determination of lipid molecules from living cells using single-cell Raman imaging. In vivo localization of lipids in the form of triacylglycerol (TAG) within oleaginous microalga and their molecular compositions are monitored with high spatial resolution in a non-destructive and label-free manner. This method can provide quantitative and real-time information on compositions, chain lengths, and degree of unsaturation of fatty acids in living cells for improving the cultivating parameters or for determining the harvest timing during large-scale cultivations for microalgal lipid accumulation toward biodiesel production. Therefore, this technique is a potential tool for in vivo lipidomics for understanding the dynamics of lipid metabolisms in various organisms.

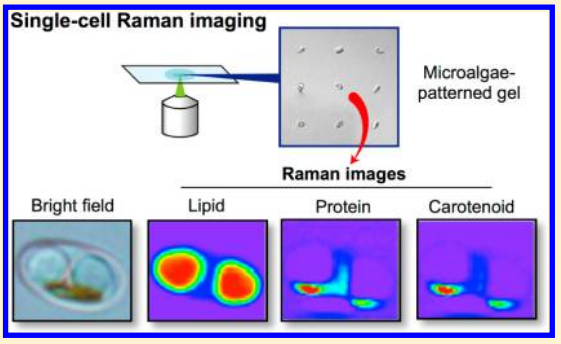

In vivo monitoring of biomolecules has proven to be a powerful analytical technique for understanding the spatiotemporal dynamics of biomolecules within the cells. In conjunction with the development of various fluorescent molecules for tracking cellular components, the heterogeneity of cellular behavior has been revealed.[1−3] Indeed, molecularly designed fluorescent proteins and fluorescently labeled nucleic acids have been widely used for in situ detection and monitoring of the dynamics of the targeted proteins, DNA, or RNA.[4,5] However, it is difficult to quantitatively determine the detailed chemical composition and metabolomics of biomolecules such as cellular lipids due to the lack of adequate tracking probes. Although sensitive lipid-soluble fluorescent probes (e.g., Nile red[6,7] and BODIPY[8]) have been utilized to observe intracellular neutral lipid localization, these fluorescent probes cannot provide the detailed chemical information on the fatty acid profiles of neutral lipids, such as the composition, degree of unsaturation, and chain length.

Lipid storage organelles exist in almost all organisms from bacteria to humans and are called oil bodies and oleosomes in the seeds of plants. Several model systems, including bacteria, fungi, microalgae, nematode (*Caenorhabditis elegans*), *Drosophila*, plant cells, and mammalian cells have been used to study the biosynthesis and function of lipid storage organelles.[9] In particular, microalgae are known to be capable of accumulating large amounts of lipids in the form of triacylglycerols (TAG): triesters of glycerol with saturated or unsaturated fatty acid, which have attracted much attention as a strategic source of biodiesel.[10−14] TAG accumulation resulted in formation of oil bodies, which were surrounded by a phospholipid monolayer.[15] Although current studies have focused mainly on the synthesis pathways for fatty acids and TAG via the chloroplast and the endoplasmic reticulum (ER) membrane,[16−18] the biosynthetic origin of TAG in most microalgae remained unclear. Understanding the in vivo lipid dynamics under TAG accumulation in oil bodies would contribute to efficient TAG production in microalgae. However, conventional analyses were commonly performed by solvent extraction-based methods coupled with gas chromatography/mass spectrometry (GC/MS), which are typically destructive and time-consuming. Moreover, the

Received: May 1, 2014
Accepted: July 29, 2014
Published: July 29, 2014

   dx.doi.org/10.1021/ac501591d | *Anal. Chem.* 2014, 86, 8224−8230

information linking cellular dynamics and functionality is often lost during the extraction step typically required for these assays, and therefore, these techniques become less useful for understanding and controlling the fundamental biological processes needed for improving TAG production. In addition, since the microalgal TAGs are the raw materials for biodiesel fuel (BDF) synthesis, it is crucial to quantify the fatty acid composition in the microalgal biomass. The European biodiesel standards EN 14214 have defined the maximum limits of fatty acid contents, i.e., fatty acid methyl ester (FAME) with more than four double bonds [<1% (w/w)], because the unsaturation grade affects the cold flow, stability, and ignition quality of diesel fuel.[19,20] Therefore, a technique capable of providing real-time information for improving the cultivating parameters or determining the harvest timing during large-scale cultivation is required to optimize the yields and quality of TAGs.

Raman spectroscopy offers an attractive tool for rapid characterization of cellular molecules, providing quantitative chemical composition in a label-free, nondestructive, and real-time manner.[21] So far, broad spectra of algal species were investigated by Raman spectroscopy for the identification of their major components: proteins, carbohydrates, lipids, nucleic acids, and pigments.[22] These studies have mainly focused on the identification of hydrocarbons or glycerolipids in algal cells including *Chlorella sorokiniana*, *Neochloris oleoabundans*, *Botryococcus braunii*, *B. sudeticus*, *Chlamydomonas reinhardtii*, and *Trachydiscus minutus* as candidates for biofuel production.[23−27] Recently, in vivo lipid profiling based on Raman spectroscopy has shown its feasibility for the nondestructive estimation of the unsaturation degree of constituent fatty acids within oil bodies of live algal cells such as *N. oleoabundans*, *B. braunii*, *B. sudeticus*, *C. reinhardtii*, and *T. minutus*.[24,25,27] However, although algae are known to show changes in composition or structure depending on the change in the environmental conditions,[10] time-dependent and quantitative analysis of lipid composition has not been achieved yet in vivo due to the lack of appropriate resolution to quantify the fatty acid profiles of TAGs conserved in single cells. Although a few studies were focused on mapping the presence and location of algal lipids within a single cell or a colony,[23,26] the imaging resolution was not adequate to identify individual organelles such as oil bodies and chloroplasts within the cells. Hence, the dynamic changes of the composition of fatty acids in TAGs and their distribution in a single cell during the TAG accumulation process are still unknown. To understand the dynamic behavior of molecular composition and distribution in single cells, we have developed a Raman imaging technique with high temporal and spatial resolutions with the aid of a confocal Raman microspectrometer equipped with a cross slit, which functions as a confocal pinhole.[28,29] Using this laboratory-built confocal Raman microspectrometer, we have recently achieved the first time-lapse Raman imaging of a single dividing *Schizosaccharomyces pombe* cell.[30−32] The obtained Raman images showed that the concentration and distribution of lipids and proteins varied in a concerted manner as the cell cycle proceeded.[30] Thus, the single-cell Raman imaging is a valuable, complementary approach for understanding both quantitatively and dynamically the molecular process that underlies single-cell activities.

In this study, in vivo live cell imaging was conducted using a laboratory-built single-cell Raman microspectrometer for the quantitative monitoring of TAGs in the oleaginous microalgae *Fistulifera solaris* JPCC DA0580 during the TAG accumulation process. This strain is a marine oleaginous diatom that is recognized as a candidate for efficient TAG production as a raw material for BDF because it is fast growing and capable of accumulating a large quantity of oil up to 60% of its dried mass.[33,34] The FAME obtained from this microalga were mainly methyl palmitate (C16:0) and methyl palmitoleate (C16:1), which have potential utility as BDF.[35] Moreover, this strain contains the polyunsaturated fatty acid eicosapentaenoic acid (EPA).[36] These fatty acids account for over 90% of the total TAG fatty acids in the oil bodies of *F. solaris* JPCC DA0580.[35,36] Recently, we performed the genetic transformation of this strain for controlling the fatty acids composition toward efficient BDF production.[37,38] Moreover, the oleaginous microalga is considered a good model for the study of in vivo lipidomics because it possesses a single chloroplast and two oil bodies inside the stiff frustules composed of SiO_2.[39] The chloroplasts are compartmentalized from the cytoplasm by four bilayer membranes, in which the two outer membranes are directly connected to the ER membranes and closely interact with the oil bodies.[18,39] This membrane complex acts as a barrier to purely separate the oil bodies from other organelles and helps us in tracking the dynamics of TAG accumulation. Indeed, the main components of the microalgal cell, such as lipids, proteins, and carotenoids, have been successfully visualized by single-cell Raman imaging based on the fingerprint region of their spectra. We revealed that the localization and the accumulation of TAGs dominantly occurred in the oil bodies under nutrient-starved conditions. Our results suggested that the proposed approach for monitoring of in vivo lipid composition has the potential for the screening of oleaginous microalgae and the optimization of the growth conditions for TAG production by providing quantitative fatty acid profiling. Furthermore, this study demonstrates the capability of the single-cell Raman imaging for investigating the dynamic behaviors of in vivo lipidomics.

EXPERIMENTAL SECTION

Strain and Culture Conditions. The stock culture of the marine oleaginous diatom *F. solaris* JPCC DA0580 was maintained in 10f medium, which contained 10 times higher nutrition components than the "f" medium.[40] For each experiment, the preculture was prepared by diluting the stock culture into the freshly prepared 10f medium (200 mL, 1.0×10^6 cells/mL) and incubating for 1 week. After preculture, two-phase cultivation was performed to induce neutral lipid accumulation in microalgal cells. For the first incubation phase, preculture cells were transferred into a flat-shaped flask containing 1.5 L of 10f medium at initial concentration of 1.0×10^6 cells/mL and cultured for approximately 72 h. Subsequently, microalgal cells were collected by centrifugation at 8000*g* for 10 min. For the second incubation phase, the collected cells were resuspended in artificial seawater without nutrient supplementation and incubated for 96 h. The temperature was maintained at 25 ± 1 °C using temperature-controlled baths. Continuous illumination was applied from one direction at 200 $\mu mol \cdot m^{-2} \cdot s^{-1}$ to the flat-shaped flasks using cool fluorescent tubes. The illumination intensity was measured by using illuminometers. The cultures were bubbled with sterile air containing 2% CO_2.

Raman Spectrometry. A 532 nm line of a Nd:YAG laser (Compass 315M, Coherent Inc., Santa Clara, CA) was used as the Raman excitation line. The laser beam was focused by a

dx.doi.org/10.1021/ac501591d | Anal. Chem. 2014, 86, 8224−8230

100×/1.4 numerical aperture (N.A.) objective lens (Plan Apo VC, Nikon Corporation, Tokyo, Japan) onto the sample placed on the stage of an inverted microscope (ECLIPSE Ti, Nikon Corporation), resulting in spatial resolution of the Raman imaging system of 0.33, 0.39, and 2.1 μm for the x, y, and z directions, respectively, at the laser focus. The backscattered Raman light was collected by the same objective lens and measured with a spectrometer (MS3504i, SOL instruments, Ltd., Minsk, Republic of Belarus, 1200 lines/mm) and a charge-coupled device (CCD) camera (Newton DU920-M, Andor Technology plc., U.K.) via the cross slit (Figure 1). See the Supporting Information for details.

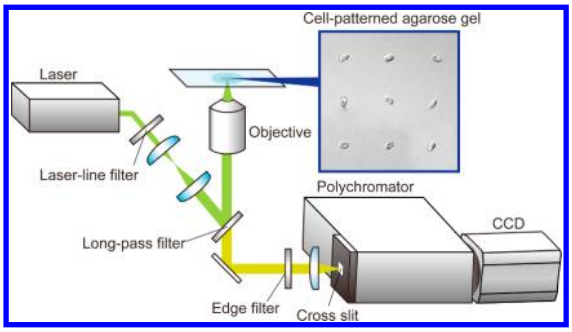

Figure 1. Schematic of the experimental setup of the single-cell Raman imaging system. The instrument layout shows the 532 nm laser used for Raman excitation, filters, objective lens, cross slit functioning as the confocal pinhole, polychromator, and charge-coupled device (CCD) camera. For immobilization of cells during laser scanning, individual microalgal cells were patterned on the agarose gel pad with 25 μm in pitch by employing the micropatterning method using a microcavity array.

Sample Preparation. Before Raman imaging, single cells were patterned on an agarose gel pad to immobilize the cell position and shorten the time required to capture the Raman and fluorescent images as described in a previous report.[41] First, the cell suspension was dropped on the microcavity array and subsequently suctioned to trap single cells on 102 400 cavities arranged in a 320 × 320 array. Microalgal cells were suspended in phosphate-buffered saline (PBS) at a concentration of approximately 5×10^3 cells/μL. The cell suspension (20 μL) was dispensed onto a PBS-filled cell-entrapment device equipped with a microcavity array. Negative pressure was then applied to the cell suspension by using a peristaltic pump connected to the vacuum line at a flow rate of 200 μL/min. After cell entrapment on the microcavities, f/2 medium with 2.0% (w/v) low-melting point (LMP) agarose at 42 °C was dropped onto the microcavity array and then left at room temperature for 15 min for gelation. The solidified agarose gel pad (8 mm × 8 mm) was then peeled off the microcavity array with tweezers and transferred to a cleaned glass bottom dish.

GC/MS. The lyophilized microalgal cells (50 mg) were suspended by using a pestle and mortar and were added to n-hexane (10 mL). After volatilization, 1.25 M HCl−methanol (5 mL) was added to the extracted lipids, and the mixture was heated at 100 °C for 1.5 h. After esterification, n-hexane (4 mL) and purified water (2.5 mL) were added, the mixture was centrifuged (6500g, 5 min), and the supernatant was collected. Distilled water was added to the supernatant, which was then recentrifuged and dried over sodium sulfate (10 mg). The evaporated, lipid fraction was resuspended in 2.5 mL of n-hexane, and the lipid components were isolated and characterized by using GC/MS (QP2010; Shimadzu Co.). The GC conditions were as follow: FAMEWAX column (30 m, 0.25 mm i.d., 0.25 μm; Restek) at an oven temperature-programmed to 140 °C for 5 min, and then to 250 °C, increasing at 4 °C/min using helium as the carrier gas. The fatty acids were identified and quantified by comparison with a FAME standard mix (FAME mix, C4−C24 unsaturates; Sigma-Aldrich).

RESULTS AND DISCUSSION

Experimental Setup of Single-Cell Raman Imaging. The single-cell Raman imaging system developed here combined the Raman microspectroscopy and the microcavity array-based single-cell patterning technique.[41,42] The laboratory-built confocal Raman microspectrometer consisted of a 532 nm laser, an inverted microscope with a 100× 1.4 N.A. lens fitted with a filter set to clean the laser and block the Rayleigh scattering, cross slit, a polychromator, and a CCD camera (Figure 1). A 50 μm × 50 μm cross slit was used as the entrance slit of the polychromator. This cross slit also functioned as the confocal pinhole, reducing the number of optics used and increasing the throughput of the Raman collection optics. For the confocal Raman spectral analysis of a point of interest within the cells, the spatial resolution of the Raman imaging system was set to be 0.33 and 2.1 μm for the lateral and depth directions, respectively. Single microalgal cells were patterned on an agarose gel pad using the microcavity-based live cell patterning technique to simplify laser scanning by arranging the cells in a spatially defined pattern and physically separating them from one another. Single cells were patterned and immobilized on a single focal plane of agarose gel, resulting in the shortening of the time required to capture the Raman and fluorescent images of the cells. Because the patterning process does not affect the cellular activity, we could individually analyze given single live cells using this system. Typical acquisition times for well-resolved spectra of pure fatty acids were 10 s and, for a microalgal cell, 2 s. For Raman imaging, the sample area was scanned at 0.25 μm pitch.

In Vivo Raman Imaging of the Cellular Components of Single Microalga Cells. To verify the performance of the in vivo Raman imaging, we first recorded the Raman spectra of the chloroplast and oil bodies of a single microalgal cell after 72 h of incubation in nutrient-depleted medium (artificial seawater). As shown in the inset of Figure 2A, almost all cytoplasm was filled with the chloroplast (yellowish-brown) and two oil bodies (transparent and spherical bodies); the localization of each organelle was readily discernible in the bright-field image. The Raman spectra obtained from each organelle showed quite different patterns (Figure 2A). In the Raman spectrum of the oil bodies, the peaks at 1266 and 1656 cm^{-1} corresponded to the cis =C−H in-plane deformation and the cis C=C stretch, respectively.[43] These two peaks provided unequivocal evidence for chain unsaturation. Moreover, the peaks at 1302 and 1445 cm^{-1} corresponded to the CH_2 twist and the CH_2 bend, respectively. These two peaks were assigned to saturated-CH_2 bonds.[27] The peak at 1742 cm^{-1}, which corresponds to ester C=O stretch, was indicative of triglyceride esterification within the oil bodies.[27] These peaks clearly indicated the presence of abundant TAGs in the oil bodies. In the Raman spectrum of the chloroplast, carotenoids could be found at 1003, 1156, and 1520 cm^{-1}, which were assigned to the C−C and the C=C stretches.[44] In addition, proteins could be found at 1003 cm^{-1}, which corresponded to

dx.doi.org/10.1021/ac501591d | Anal. Chem. 2014, 86, 8224−8230

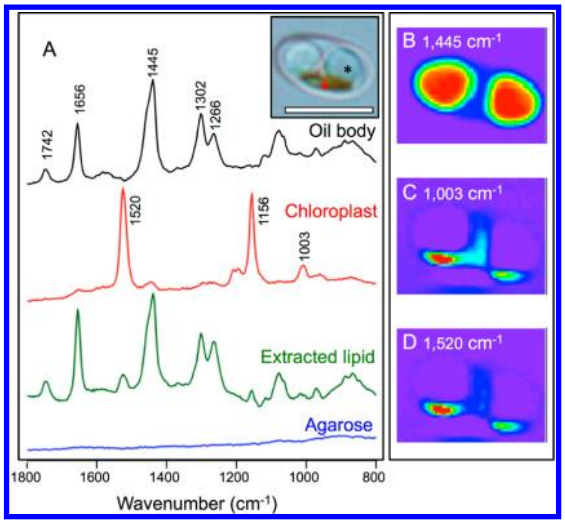

Figure 2. Single-cell Raman image analysis of an oil body in *F. solaris* JPCC DA0580. (A) Raman spectra of oil bodies, chloroplast, extracted lipid, and agarose gel. The inset shows the bright-field image of a *F. solaris* JPCC DA0580 cell after 72 h of cultivation in nutrient-depleted medium. The red and black asterisks indicate the chloroplast and the oil bodies, respectively, in the single cell. Scale bar: 5 μm. (B–D) Raman images of a *F. solaris* JPCC DA0580 cell at (B) 1445 cm^{-1} (lipid), (C) 1003 cm^{-1} (protein and carotenoid), and (D) 1520 cm^{-1} (carotenoid).

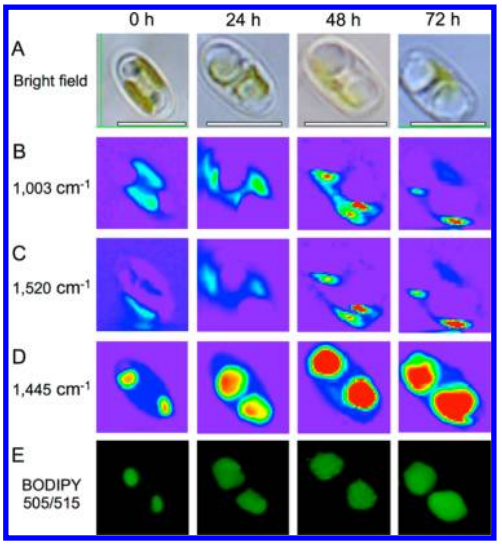

Figure 3. Gallery of Raman images and fluorescent images obtained at different time points after lipid accumulation induction. (A) Bright-field image of *F. solaris* JPCC DA0580. Scale bar: 5 μm. (B–D) Raman images at (B) 1003 cm^{-1} (carotenoid and protein), (C) 1520 cm^{-1} (carotenoid), and (D) 1445 cm^{-1} (lipid). (E) Fluorescent images of cells stained with BODIPY 505/515.

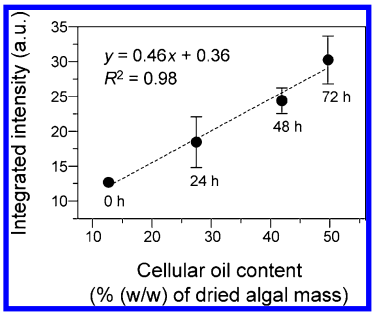

Figure 4. Relationships between the cellular oil contents and the integrated Raman intensity at 1445 cm^{-1} (lipid). The oil content and the Raman intensity were measured by GC/MS and Raman microspectrometry, respectively, in the same culture sample of *F. solaris* JPCC DA0580 under TAG accumulation condition at 0, 24, 48, and 72 h. The integrated Raman intensities are represented as mean ± standard error.

the phenylalanine ring breath.[30] No obvious peaks were observed from background agarose gel (Figure 2A).

To visualize the distribution of the major cellular components, the Raman images of lipids (1445 cm^{-1}), carotenoids (1003 and 1520 cm^{-1}), and proteins (1003 cm^{-1}) were constructed (Figure 2B–D). The lipids of *F. solaris* JPCC DA0580 were locally conserved in the two oil bodies at high concentration, while carotenoids were outside of the two oil bodies. Although some algae strains such as *T. minutus* contain β-carotene in high amounts in their oil bodies,[44] based on the in vivo Raman spectrum profiling, carotenoids of *F. solaris* were isolated in the outside of the oil bodies. Moreover, the Raman spectrum of the extracted algal lipids was compared to that of intact oil bodies and chloroplasts. After 72 h of cultivation in nutrient-depleted medium, the algal lipids were extracted from *F. solaris* JPCC DA0580 using *n*-hexane. As shown in Figure 2A, the peaks assigned to both lipids and carotenoids could be found in the spectrum of the extracted lipids. Thus, we considered that some carotenoids might be mixed in the lipid fraction during the lipid extraction process. The Raman imaging technique presented here allows the localization of intact lipids stored in oil bodies without labeling or extraction.

Time-Dependent Analysis of the Oil Bodies by Raman Imaging and Estimation of the Oil Content from the Raman Intensity. To determine the dynamic changes of the TAG accumulation process, a two-phase cultivation was performed to induce neutral lipid accumulation in microalgal cells. We obtained the Raman spectra of single microalgal cells 0–72 h after the incubation in nutrient-depleted medium (artificial seawater), and the Raman images at 1445 cm^{-1} (lipid), 1003 cm^{-1} (carotenoid and protein), and 1520 cm^{-1} (carotenoid) were constructed at each time point (Figure 3). The cellular oil contents in the extracted lipids, measured by GC/MS, reached >40% of the dried algal mass after 48 h of cultivation (Figure 4). The time-series Raman images show the expansion of the lipid area, while the areas of the carotenoids and proteins narrowed down at the edge of the cellular cytoplasm with the increasing of the Raman intensities (Supporting Information Figure S-1). On the basis of the different distributions of the lipids conserved in the oil bodies and constituent proteins and carotenoids in the chloroplast, we could discriminate the time-dependent changes in the structures of the oil bodies and chloroplast during the TAG accumulation process. Since the spatial resolution of Raman imaging is smaller than the dimension of the cell, the Raman intensity mapping depended on constituent molecules within the focal points and implied the three-dimensional structure of the chloroplast surrounding the oil bodies. According to the Raman images of each cellular component, the enlarged oil bodies might push the cytoplasmic components and chloroplast onto the edge of the cells, even though the distributions of carotenoids and proteins originally differed from one another.

To confirm the lipid distribution within the cell, the same cells were stained with BODIPY 505/515, a lipophilic bright

dx.doi.org/10.1021/ac501591d | Anal. Chem. 2014, 86, 8224–8230

green fluorescent dye used for the detection of intracellular neutral lipids. The distribution of lipids shown in the Raman image (Figure 3) was consistent with the bright-field and fluorescent images of the cells stained with BODIPY 505/515. In conjunction with the Raman images, the relationship between cellular oil contents measured by GC/MS from extracted lipids and Raman intensities integrated over the whole cell (Supporting Information Figure S-1) was evaluated at each time point. As shown in Figure 4, the curve indicated that the integrated Raman intensity at 1445 cm^{-1} and oil content in the extracted lipid measured by GC/MS were highly correlated. This result suggested that the oil content could be quantitatively determined from the integrated Raman intensities of single cells. The continuous increase of the integrated Raman intensity at 1445 cm^{-1} during the TAG accumulation process (Figure 3 and Supporting Information Figure S-1) was also correlated with the expansion of the lipid area in the Raman image.

Quantitative Analysis of in Vivo Lipid Unsaturation. Previous studies showed that changes in the ratio of the peak intensities at 1656 and 1445 cm^{-1} correlated with the number of double bonds presents in the fatty acids and reflected the total degree of unsaturation.[24,27] These marker peaks are proportional to the amount of unsaturated C═C bonds and saturated C−C bonds, respectively. To build the foundation for the quantitative analysis of the unsaturation degree of fatty acids consist of algal lipids, we performed a series of Raman spectroscopic measurements of pure fatty acids of different degrees of unsaturation by using our Raman microspectrometer. Several specific Raman markers, directly associated with lipid saturation or unsaturation, were observed in the Raman spectra shown in Supporting Information Figure S-2. As shown in Figure 5A, the ratio of the Raman intensity of the C═C

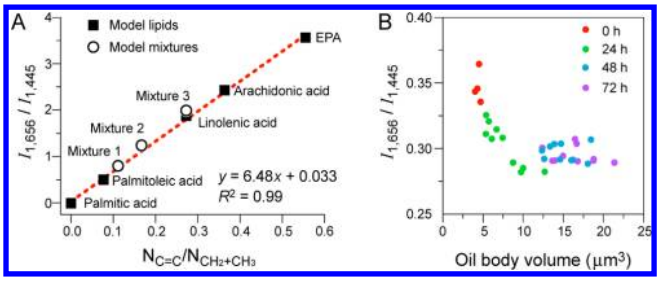

Figure 5. Quantitative analysis of the degree of unsaturation of the standard fatty acids and algal lipids in the oil bodies. (A) Calibration curve for the estimate of the degree of unsaturation from Raman spectral data. I_{1656}/I_{1445} of the standard fatty acids are plotted vs the number of C═C bonds per molecule and fitted linearly to predict the degree of unsaturation of the extracted algal lipids and lipids in the oil bodies. (B) Relationships between the size and the I_{1656}/I_{1445} ratio of the oil bodies in *F. solaris* JPCC DA0580.

stretch to the intensity of CH_2 and CH_3 deformation (I_{1656}/I_{1445}) displays a linear dependence with the ratio of the number of C═C bonds to the number of CH_2 and CH_3 groups ($N_{C=C}/N_{CH2+CH3}$) for standard fatty acids. To verify the validity of this calibration curve for the determination of the degree of unsaturation, we performed additional spectroscopic measurements with binary mixtures of EPA and palmitoleic acids of two different molar ratios (i.e., EPA:palmitoleic acid = 1:1, 1:3, and 1:9). I_{1656}/I_{1445} of these model mixtures showed clear correlation with their $N_{C=C}/N_{CH2+CH3}$ value (Figure 5A). Thus, we concluded that the calibration curve could be adopted for the characterization of the degree of unsaturation of TAGs in the microalgal cell.

On the basis of this ratiometric analysis, we evaluated the relationships between oil body size and lipid unsaturation. The I_{1656}/I_{1445} ratio was measured from the Raman spectra obtained from the oil bodies of intact single cells during the TAG accumulation process. Moreover, the sizes of the same oil bodies were measured by using a confocal fluorescent microscope. After the acquisition of the Raman spectra, the same microalgal cells were stained with BODIPY 505/515, followed by the acquisition of the confocal fluorescence images. The volumes of individual oil bodies were calculated from the sliced images. Both Raman and fluorescence image acquisitions of the same single cells were successfully performed with the aid of the single-cell array on agarose gel, which enables us to immobilize cells at an addressable position. As shown in Figure 5B, the volumes of the oil bodies significantly increased until 48 h of cultivation in nutrient-depleted medium. The I_{1656}/I_{1445} ratio of the oil bodies decreased with the increase of their volume and reached a plateau after 48 h of cultivation. This result indicated that the saturated fatty acids were preferentially synthesized and stored as TAG in the oil bodies during the nutrient-depleted phase, resulting in the decrease of the I_{1656}/I_{1445} ratio of the oil bodies. These results agree well with the previous analytical data determined by GC/MS.[35] In addition, to verify the variations between the oil bodies, we visualized the distribution of the degree of unsaturation of constituent lipids within the single cells (Supporting Information Figure S-3). Although two oil bodies usually show similar size and distribution of unsaturated lipids in most cells, a small number of cells possessed heterogeneously sized oil bodies. These heterogeneously sized oil bodies showed differences in the degree of unsaturation, which agreed with the relationship between oil body size and degree of unsaturation of lipids accumulated in the oil body (Figure 5B). Thus, our Raman imaging technique enables us not only to provide lipid distribution but also to elucidate the compositional distribution of the lipids conserved in the oil bodies with high spatial distribution.

Quantitative Analysis of Fatty Acid Composition. As described in previous reports,[35,36] the major fatty acids of *F. solaris* JPCC DA0580 are palmitate (C16:0), palmitoleate (C16:1), and EPA (C20:5). The content of 16:0 and 16:1 fatty acids increased to nearly 90% (w/w) during cultivation. However, the above information was obtained from the extracted algal lipid by using GC/MS. In vivo quantitative profiling of fatty acid composition has not been achieved yet. To elucidate the composition of the fatty acids stored as TAG in the oil bodies by using Raman spectrometry, we fitted the spectra using the least-squares method. To build the foundation for quantitative fitting analysis of fatty acid composition, we utilized a series of Raman spectra of pure fatty acids stored in the oil bodies as major components. The compositional ratio of fatty acids in algal lipid was calculated from the coefficients of the linear combination of the least-squares fitting according to the spectra of pure fatty acids. The fitted spectrum was processed by using the least-squares method in the region containing the Raman markers associated with lipid saturation or unsaturation (1048−1112, 1215−1508, and 1640−1722 cm^{-1}). First, we evaluated the accuracy of the fitting analysis in model fatty acid mixture samples. As shown in Supporting Information Figure S-4A−C, a typical preprocessed spectrum and the corresponding fitted spectrum look nearly identical;

dx.doi.org/10.1021/ac501591d | *Anal. Chem.* 2014, 86, 8224−8230

Table 1. Fatty Acid Compositions Analyzed by GC/MS and Raman Fitting Analysis[a]

condition	method	fatty acid composition (%)		
		C16:0	C16:1	C20:5n3
extracted lipid	GC/MS	45.6 (±0.3)	49.6 (±0.3)	4.8 (±0.1)
extracted lipid	Raman fitting	46.0 (±2.3)	49.4 (±2.8)	4.6 (±0.6)
in vivo (oil body)	Raman fitting	41.2 (±0.7)	55.5 (±0.7)	3.3 (±0.4)

[a]After 72 h of cultivation under nutrient-depleted condition, *F. solaris* JPCC DA0580 cells were analyzed by Raman microspectroscopy. Extracted lipids were obtained from the same culture and analyzed accordingly.

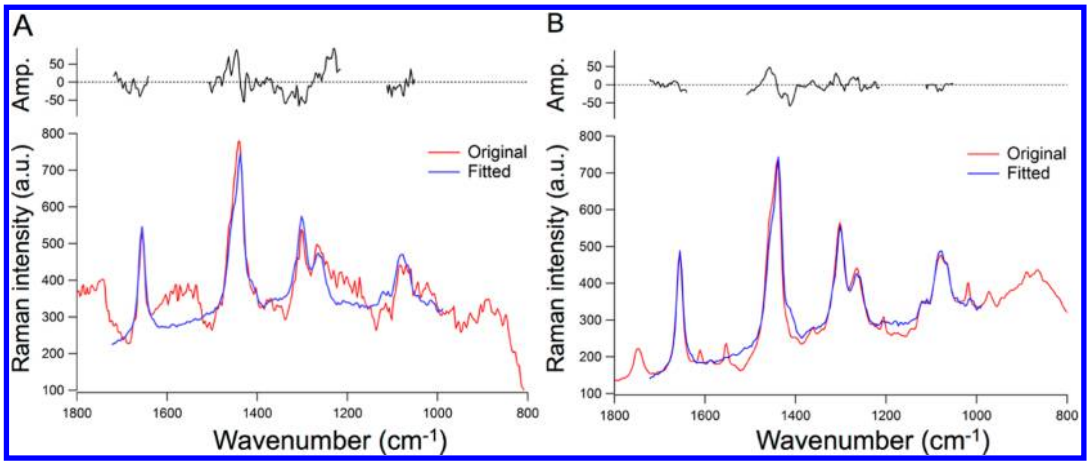

Figure 6. Raman fitting analysis for lipid composition profiling. Direct Raman fitting analysis of extracted lipids (A) and in vivo (oil body) (B) of *F. solaris* JPCC DA0580 cells after 72 h of cultivation under nutrient-depleted condition. The upper panels represent the residual errors.

their difference spectrum shows a fitting residue of less than 5%. The compositional ratios determined from the fitted spectrum agreed with the theoretical ratio (Supporting Information Table S-1). Second, the compositional ratios of the extracted lipid from GC/MS and Raman spectra fitting analysis were compared (Table 1). The algal lipid fraction was extracted from *F. solaris* JPCC DA0580 after 72 h of lipid accumulation and purified as fatty acid methyl ester. The same extracted algal lipid samples were analyzed by GC/MS and Raman fitting analysis (Figure 6A) side by side. No significant differences were observed in the compositional ratios of each fatty acid in the extracted lipid, even though the standard deviation of the Raman fitting due to fitting error was slightly larger than that of GC/MS. Therefore, we concluded that the Raman fitting analysis could provide reliable information on the component ratio of the major fatty acids in algal lipids. On the basis of these findings, we utilized this method against intact oil bodies in live cells (Figure 6B). The Raman spectra of the oil body area within intact cells were obtained after 72 h of TAG accumulation. As shown in Table 1, palmitate (C16:0) and EPA (C20:5) ratios of intact cells (41.2% ± 0.7% and 3.3% ± 0.4%, respectively) were relatively low compared to those of the extracted lipid (46.0% ± 2.3% and 4.6% ± 0.6%, respectively), while the palmitolate ratio of intact cells (55.5% ± 2.3%) was higher than that of the extracted lipid (49.4% ± 2.8%). These differences were therefore considered due to the contamination of polar lipids bound to membrane proteins into the extracted lipids. In support of this consideration, the Raman spectrum of intact oil body showed lower background signal than that of the extracted algal lipids, thus resulting in small residual error in the difference spectrum (Figure 6, parts A and B). The residual errors in the difference spectrum of the extracted lipid (Figure 6A) indicated the contamination of some biomolecules. As described in previous reports,[45,46] the amount and the content of fatty acids in the extracted algal lipids highly depend on the physical and chemical extraction conditions such as solvent, temperature, pressure, and pH. Hence, GC/MS, whose results depend on the lipid extraction condition, might overestimate or underestimate the compositional ratio of the unsaturated fatty acid EPA in the oil bodies. Indeed, as described above, the Raman spectrum of the oil bodies (Figure 6B) dominantly showed lipid-specific bands. We considered that the compositional ratio of the fatty acids analyzed by Raman microspectroscopy provided information in vivo on molecules that had been obscured in conventional GC/MS analysis.

CONCLUSIONS

In this study, we demonstrated that single-cell Raman imaging could provide a rapid and quantitative characterization of fatty acid profiles of storage lipids from single microalgae cells in a nondestructive and label-free manner. The time-dependent changes of the composition and in vivo localization of lipids were clearly observed at the single-cell level by using this technique. The correlation between algal oil content measured by GC/MS and Raman intensities could facilitate rapid in vivo quantification of oil productivity for high-throughput screening of oleaginous microalgae. Moreover, the Raman fitting analysis provided a detailed composition of fatty acid, which consist of TAGs in the oil body. The fatty acid composition profile could be obtained from intact oil bodies conserved in live cells without biases arising from the lipid extraction process. Our results suggested that single-cell Raman imaging could provide intact molecule information from live single cells due to its destruction-independent analysis manner. Therefore, this technique would facilitate the routine assessment of algal growth and lipid productivity and the development of an effective lipid extraction process in industrial scale.

dx.doi.org/10.1021/ac501591d | *Anal. Chem.* 2014, 86, 8224−8230

■ ASSOCIATED CONTENT

Supporting Information

Additional information as noted in text. This material is available free of charge via the Internet at http://pubs.acs.org.

■ AUTHOR INFORMATION

Corresponding Authors

*Phone: +886-3-5712121. Fax: +886-3-5723764. E-mail: hhama@nctu.edu.tw.

*Phone: +81-42-388-7401. Fax: +81-42-385-7713. E-mail: tsuyo@cc.tuat.ac.jp.

Author Contributions

⊥M.H. and M.A. contributed equally to this work.

Notes

The authors declare no competing financial interest.

■ ACKNOWLEDGMENTS

This study was supported by JST-CREST and JSPS KAKENHI Grant No. 23360363.

■ REFERENCES

(1) Nebe-von-Caron, G.; Stephens, P. J.; Hewitt, C. J.; Powell, J. R.; Badley, R. A. *J. Microbiol. Methods* **2000**, *42*, 97−114.

(2) Davey, H. M.; Kell, D. B. *Microbiol. Rev.* **1996**, *60*, 641−696.

(3) Joux, F.; Lebaron, P. *Microbes Infect.* **2000**, *2*, 1523−1535.

(4) Zhang, J.; Campbell, R. E.; Ting, A. Y.; Tsien, R. Y. *Nat. Rev. Mol. Cell Biol.* **2002**, *3*, 906−918.

(5) Elowitz, M. B.; Levine, A. J.; Siggia, E. D.; Swain, P. S. *Science* **2002**, *297*, 1183−1186.

(6) Elsey, D.; Jameson, D.; Raleigh, B.; Cooney, M. J. *J. Microbiol. Methods* **2007**, *68*, 639−642.

(7) Huang, G. H.; Chen, G.; Chen, F. *Biomass Bioenergy* **2009**, *33*, 1386−1392.

(8) Cooper, M. S.; Hardin, W. R.; Petersen, T. W.; Cattolico, R. A. *J. Biosci. Bioeng.* **2010**, *109*, 198−201.

(9) Ding, Y. F.; Zhang, S. Y.; Yang, L.; Na, H. M.; Zhang, P.; Zhang, H. N.; Wang, Y.; Chen, Y.; Yu, J. H.; Huo, C. X.; Xu, S. M.; Garaiova, M.; Cong, Y. S.; Liu, P. S. *Nat. Protoc.* **2013**, *8*, 43−51.

(10) Breuer, G.; Lamers, P. P.; Martens, D. E.; Draaisma, R. B.; Wijffels, R. H. *Bioresour. Technol.* **2012**, *124*, 217−226.

(11) Rodolfi, L.; Zittelli, G. C.; Bassi, N.; Padovani, G.; Biondi, N.; Bonini, G.; Tredici, M. R. *Biotechnol. Bioeng.* **2009**, *102*, 100−112.

(12) Schenk, P. M.; Thomas-Hall, S. R.; Stephens, E.; Marx, U. C.; Mussgnug, J. H.; Posten, C.; Kruse, O.; Hankamer, B. *BioEnergy Res.* **2008**, *1*, 20−43.

(13) Smith, V. H.; Sturm, B. S.; Denoyelles, F. J.; Billings, S. A. *Trends Ecol. Evol.* **2010**, *25*, 301−309.

(14) Hu, Q.; Sommerfeld, M.; Jarvis, E.; Ghirardi, M.; Posewitz, M.; Seibert, M.; Darzins, A. *Plant J.* **2008**, *54*, 621−639.

(15) Murphy, D. J. *Prog. Lipid Res.* **2001**, *40*, 325−438.

(16) Fan, J.; Andre, C.; Xu, C. *FEBS Lett.* **2011**, *585*, 1985−1991.

(17) Goodson, C.; Roth, R.; Wang, Z. T.; Goodenough, U. *Eukaryotic Cell* **2011**, *10*, 1592−1606.

(18) Liang, Y.; Maeda, Y.; Sunaga, Y.; Muto, M.; Matsumoto, M.; Yoshino, T.; Tanaka, T. *Mar. Drugs* **2013**, *11*, 5008−5023.

(19) Durrett, T. P.; Benning, C.; Ohlrogge, J. *Plant J.* **2008**, *54*, 593−607.

(20) Knothe, G. *J. Am. Oil Chem. Soc.* **2006**, *83*, 823−833.

(21) Krafft, C.; Dietzek, B.; Popp, J. *Analyst* **2009**, *134*, 1046−1057.

(22) Parab, N.; Tomar, V. *J. Nanomed. Nanotechnol.* **2012**, *3*, 2.

(23) Huang, Y. Y.; Beal, C. M.; Cai, W. W.; Ruoff, R. S.; Terentjev, E. M. *Biotechnol. Bioeng.* **2010**, *105*, 889−898.

(24) Samek, O.; Jonas, A.; Pilat, Z.; Zemanek, P.; Nedbal, L.; Triska, J.; Kotas, P.; Trtilek, M. *Sensors* **2010**, *10*, 8635−8651.

(25) Samek, O.; Zemanek, P.; Jonas, A.; Telle, H. H. *Laser Phys. Lett.* **2011**, *8*, 701−709.

(26) Weiss, T. L.; Chun, H. J.; Okada, S.; Vitha, S.; Holzenburg, A.; Laane, J.; Devarenne, T. P. *J. Biol. Chem.* **2010**, *285*, 32458−32466.

(27) Wu, H.; Volponi, J. V.; Oliver, A. E.; Parikh, A. N.; Simmons, B. A.; Singh, S. *Proc. Natl. Acad. Sci. U. S. A.* **2011**, *108*, 3809−3814.

(28) Huang, Y. S.; Karashima, T.; Yamamoto, M.; Hamaguchii, H. *J. Raman Spectrosc.* **2003**, *34*, 1−3.

(29) Huang, Y. S.; Karashima, T.; Yamamoto, M.; Hamaguchi, H. *Biochemistry* **2005**, *44*, 10009−10019.

(30) Huang, C. K.; Ando, M.; Hamaguchi, H.; Shigeto, S. *Anal. Chem.* **2012**, *84*, 5661−5668.

(31) Huang, C. K.; Hamaguchi, H.; Shigeto, S. *Chem. Commun. (Cambridge, U. K.)* **2011**, *47*, 9423−9425.

(32) Kano, H.; Hamaguchi, H. *Anal. Chem.* **2007**, *79*, 8967−8973.

(33) Matsumoto, M.; Sugiyama, H.; Maeda, Y.; Sato, R.; Tanaka, T.; Matsunaga, T. *Appl. Biochem. Biotechnol.* **2010**, *161*, 483−490.

(34) Matsumoto, M.; Mayama, S.; Nemoto, M.; Fukuda, Y.; Muto, M.; Yoshino, T.; Matsunaga, T.; Tanaka, T. *Phycol. Res.* **2014**, in press.

(35) Satoh, A.; Ichii, K.; Matsumoto, M.; Kubota, C.; Nemoto, M.; Tanaka, M.; Yoshino, T.; Matsunaga, T.; Tanaka, T. *Bioresour. Technol.* **2013**, *137*, 132−138.

(36) Liang, Y.; Maeda, Y.; Yoshino, T.; Matsumoto, M.; Tanaka, T. *J. Appl. Phycol.* **2014**, 1−8.

(37) Muto, M.; Fukuda, Y.; Nemoto, M.; Yoshino, T.; Matsunaga, T.; Tanaka, T. *Mar. Biotechnol.* **2013**, *15*, 48−55.

(38) Muto, M.; Kubota, C.; Tanaka, M.; Satoh, A.; Matsumoto, M.; Yoshino, T.; Tanaka, T. *PloS One* **2013**, *8*, e73507.

(39) Nojima, D.; Yoshino, T.; Maeda, Y.; Tanaka, M.; Nemoto, M.; Tanaka, T. *J. Proteome Res.* **2013**, *12*, 5293−5301.

(40) Guillard, R. R.; Ryther, J. H. *Can. J. Microbiol.* **1962**, *8*, 229−239.

(41) Osada, K.; Hosokawa, M.; Yoshino, T.; Tanaka, T. *Analyst* **2014**, *139*, 425−430.

(42) Hosokawa, M.; Arakaki, A.; Takahashi, M.; Mori, T.; Takeyama, H.; Matsunaga, T. *Anal. Chem.* **2009**, *81*, 5308−5313.

(43) Sadeghi-jorabchi, H.; Wilson, R. H.; Belton, P. S.; Edwardswebb, J. D.; Coxon, D. T. *Spectrochim. Acta, Part A* **1991**, *47*, 1449−1458.

(44) Pilat, Z.; Bernatova, S.; Jezek, J.; Sery, M.; Samek, O.; Zemanek, P.; Nedbal, L.; Trtilek, M. *J. Appl. Phycol.* **2012**, *24*, 541−546.

(45) Samori, C.; Torri, C.; Samori, G.; Fabbri, D.; Galletti, P.; Guerrini, F.; Pistocchi, R.; Tagliavini, E. *Bioresour. Technol.* **2010**, *101*, 3274−3279.

(46) Halim, R.; Danquah, M. K.; Webley, P. A. *Biotechnol. Adv.* **2012**, *30*, 709−732.